Localized description of band structure effects on Li atom interaction with graphene

Marcelo A. Romero,[1] A. Iglesias-García,[1] and E. C. Goldberg[1,2]

[1]*Instituto de Desarrollo Tecnológico para la Industria Química (INTEC-CONICET-UNL) Güemes 3450, CC91, (S3000GLN) Santa Fe, Argentina*

[2]*Departemento Ingeniería de Materiales, Facultad Ingeniería Química, U.N.L., (S3000GLN) Santa Fe, Argentina*

(Received 22 October 2010; revised manuscript received 23 December 2010; published 18 March 2011)

We study theoretically the localized aspects of the interaction between an Li atom and graphene. To this end, we use an *ab initio* calculation of the Hamiltonian terms within the Anderson model that allows us to take into account the chemical properties of Li and C atoms and the two-dimensional band structure of graphene. In this way, physical magnitudes of interest such as the hybridization function, the adatom spectral density and valence occupation are calculated. We find that the interference between the adatom neighboring sites together with the pronounced energy gap around the Γ point lead to negligible hybridization widths in a wide range of energies and are practically not dependent on the adsorption site. Consequently, this very weak coupling regime makes possible a local magnetic moment formation. Moreover, the strong suppression of the atom level broadening allows for an explanation of the unexpected neutralization measured at low energies in experiments of Li^+ scattering by a highly oriented pyrolytic graphite surface.

DOI: 10.1103/PhysRevB.83.125411 PACS number(s): 73.20.Hb, 68.43.−h, 34.70.+e, 34.35.+a

I. INTRODUCTION

The study of graphene has been motivated mostly by the unusual nature of its effectively massless charge carriers, the so-called Dirac fermions, that leads to exotic electronic properties whose potential application for future nanometer-scale devices is under extensive exploration.[1] Although clean bulk graphene may not be magnetic, there is a rich variety of possibilities for magnetism when adatoms are added on top of graphene. As an open surface, the use of scanning tunneling microscopy (STM) probes[2–4] allows for controlling the position of adatoms with atomic precision[5] and at the same time switching the magnetic local moments on and off by gating.[6,7] Several previous theoretical studies based on first-principles density-functional theory have been performed to provide an atomic level understanding of the interactions between adatoms and graphene. These works focused on the stable configurations of alkali and transition metal adatoms on graphene,[8–14] charge transfer between graphene and metals,[15] and magnetism.[16] It was found that the adatoms studied from groups I to III of the Periodic Table present ionic bonding, and the adsorption is characterized by minimal change in the graphene electronic states and large charge transfer. While for transition, noble, and group IV metals, the bonding is covalent, and the adsorption is characterized by strong hybridization between adatom and graphene electronic states.

On the other hand, the spectral, thermodynamic and scattering properties of a resonant *s-wave* magnetic impurity absorbed on clean graphene have been studied by using the Anderson Hamiltonian as the starting point.[17,18] Very simple parametrizations allowed for the description of the anomalous level broadening of the adatom when it hybridizes equally with the two graphene sublattices.[18] In addition, a model discussion based on the Anderson impurity coupled to an electron bath with linearly vanishing density of states at the Fermi level leads to Fano line shapes strongly different from the antiresonances usually found on metal surfaces. Furthermore, a realistic estimation of the Fano q factors for Co on graphene and Co on Cu(111) was obtained from density-functional calculations of the hybridization functions.[19]

In this work we investigate theoretically the interaction of atoms with graphene within the Anderson model framework. Physical quantities of interest such as hybridization functions and the spectral properties of the combined system can be straightfordwardly obtained from this model,[20–23] but a quantitative determination of the physical magnitudes depends strongly on how realistic the Hamiltonian parameters are. We use in the present work a previously developed *ab initio* calculation of the Anderson Hamiltonian terms, widely proved in several atom-surface interacting systems.[24–28] In this model calculation the hybridization term is basically determined by the extended features of the electronic band structure of the solid and the localized nature of atom-atom interactions. In this sense, graphene is an ideal surface to treat because of its simple two-dimensional band structure that makes possible a tight-binding analytical calculation of the eigenstates in the case of only considering the π band. Within this description, the interference between the different quantum mechanical paths involving the adatom neighboring sites is easily taken into account for the calculation of the Anderson hybridization function.[29] This function is a clue magnitude that allows us to infer on the characteristics of the charge exchange between atoms and surfaces in both adsorption and collision processes. Specifically, the adatom level broadening, the spectral properties, and the possibility of a local magnetic moment are intimately related to the hybridization function. In this paper we address the particular case of an Li atom interacting with graphene. The stable configuration of Li on graphene has been studied by several previous authors[8,9,14] and it was found for 50% coverage that the hollow site is lower in energy compared to the on-top site by only 0.046 eV (Ref. 14). Furthermore, Chan *et al.* (Ref. 9) concluded that the binding was ionic in nature with charge transferred from the Li to the graphene substrate without significant change to the occupied graphene bands.

Our work is mainly motivated by recent ion-surface scattering experiments. Large neutral fractions were found in

 ©2011 American Physical Society

the scattering of Li positive ions by a high oriented pyrolitic graphite (HOPG) surface.[28] The high neutralization has been explained by the pronounced downshift of the Li ionization level caused by the interaction with many atoms of the surface. The Li positive ion is efficiently neutralized along the incoming trajectory. As the atom motion leaving the surface is slower, the electron loss to the empty band states is more probable. Therefore, one would expect a decreasing neutral fraction at low ion energies. This is not the experimental result found, instead a nearly constant neutral fraction is observed at low values of the velocity component normal to the surface.[28] On the other hand, the increasing neutralization at low energies found in the scattering of Li positive ions by a Cu(111) surface[30] has been associated with the presence of surface energy band gaps.[31] In fact, this collisional system has been discussed within the Anderson model framework by using a simple tight-binding model of the solid.[32] It was found that the presence of a surface gap maximum at the Γ point and the Fermi level located inside it lead to a suppression of the hybridization function in the vicinity of the Fermi energy. We find a similar result in the case of Li interacting with graphene, but in this combined system the energy gap has a more dramatic effect on the hybridization width due to the two-dimensional crystal structure of the surface.

The present manuscript is organized in the following way. In Sec. II the Anderson interaction model is presented. Afterward, the *ab initio* calculation of the Hamiltonian terms and the tight-binding model for calculating the eigenstates and eigenenergies of graphene are briefly discussed. Finally in this section, we introduce the calculation of the local density of states (LDOS) on the adatom. Section III is devoted to the discussion of the results concerning with the hybridization width, the spectral properties, the adatom valence occupation and the neutral fraction in a time-dependent collisional process. Section IV contains the conclusions.

II. THEORY

A. Interaction model

We want to describe the three possible charge states of the Li atom (positive, neutral, and negative) when the valence $2s$- is only considered. In this case the Anderson model Hamiltonian is the adequate one for describing the interaction with the surface

$$\hat{H} = \sum_{\vec{k}n,\sigma} \epsilon_{\vec{k}n,\sigma} \hat{n}_{\vec{k}n,\sigma} + \sum_{\sigma} \left(\epsilon_a + \frac{1}{2} U \hat{n}_{a\bar{\sigma}} \right) \hat{n}_{a\sigma} + \sum_{\vec{k}n,\sigma} \left(V^{\sigma}_{\vec{k}n,a} \hat{c}^{\dagger}_{\vec{k}n,\sigma} \hat{c}_{a,\sigma} + \text{H.c.} \right). \quad (1)$$

In the second quantization language used, $\hat{c}^{\dagger}_{a,\sigma}$ creates one electron in the unique atomic orbital a considered with spin projection σ and energy ε_a, $\hat{c}^{\dagger}_{\vec{k}n,\sigma}$ creates one electron in the n-band state with wave vector $\vec{k}$ and spin projection σ and energy $\varepsilon_{\vec{k}n,\sigma}$; $\hat{n}_{a,\sigma} = \hat{c}^{\dagger}_{a,\sigma} \hat{c}_{a,\sigma}$, $\hat{n}_{\vec{k}n,\sigma} = \hat{c}^{\dagger}_{\vec{k}n,\sigma} \hat{c}_{\vec{k}n,\sigma}$ are the number operators associated with the atomic orbital and the band conduction states of the solid, respectively. The main ingredients involved in the Anderson Hamiltonian are a localized level with energy ε_a corresponding to the outermost atomic shell, an on-site repulsion U representing the screened Coulomb repulsion between a pair of electrons in the outermost shell, and a hybridization matrix element $V^{\sigma}_{\vec{k}n,a}$ between the atomic state and the conduction states of the metal. An important quantity in the Anderson model is the hybridization width defined by the expression:

$$\Gamma^{\sigma}_{a}(\varepsilon) = \pi \sum_{\vec{k}n} \left| V^{\sigma}_{\vec{k}n,a} \right|^2 \delta(\varepsilon - \varepsilon_{\vec{k}n,\sigma}). \quad (2)$$

The physics of the Anderson impurity model depends continuously on the interplay between the hybridization width and the interconfiguration energies ε_a and $\varepsilon_a + U$. The hybridization width $\Gamma^{\sigma}_{a}(\varepsilon)$ is the imaginary part of the adsorbate self-energy

$$\Xi_{0\sigma}(\omega) = \sum_{\vec{k}n} \frac{\left| V^{\sigma}_{\vec{k}n,a} \right|^2}{\omega - \varepsilon_{\vec{k}n,\sigma} + i\eta},$$

in the $U = 0$ case. In this very simple case the real part of $\Xi_{0\sigma}(\omega)$, evaluated in $\omega = \varepsilon_a$, provides the atomic level shift caused by the interaction with the band states; and the hybridization width evaluated in the shifted atom energy $\tilde{\varepsilon}_a = \varepsilon_a + \text{Re}\Xi_{0\sigma}(\varepsilon_a)$ measures the energy half-width of the atomic resonance. These concepts continue being valid in the interacting case ($U \neq 0$) provided the adsorbate self-energy can be assumed as $\Xi_{\sigma}(\omega) = \Xi_{0\sigma}(\omega) + \Xi^{\text{U}}_{\sigma}(\omega)$. Therefore, the full potentiality of the Anderson model depends on a realistic calculation of the hybridization matrix element $V^{\sigma}_{\vec{k}n,a}$.

B. Calculation of Hamiltonian terms by using the bond-pair model

We used in this work a model Hamiltonian that was previously developed to describe pairs of interacting atoms[24] and then generalized to any atom-surface system by assuming that one of the two atoms consists of a system having a quasicontinuum of states. A symmetrically orthoghonalized[33] mixed basis set of localized adatom orbitals and extended surface states is used in this case to finally reduce the Hamiltonian to the form of the Anderson model.[25] The one-electron hybridization term $V^{\sigma}_{\vec{k}n,a}$ includes one and two electron contributions determined by performing a mean field approximation together with an overlap expansion of the many body Hamiltonian. Basically the $V^{\sigma}_{\vec{k}n,a}$ term is expanded accordingly to the overlap expansion of the orthogonal $\vec{k}$ and a states. Afterward, a linear combination of atomic orbitals (LCAO) expansion of the nonperturbed $\vec{k}$-surface states is performed by approximating the three-center integrals consistently with the overlap expansion. In this way the nondimeric contributions are canceled and finally, the hybridization term is recovered as a superposition of the atomic hopping integrals $V^{\sigma(\text{dim})}_{i,\vec{R}_S,a}$ calculated with functions only orthogonalyzed within each dimeric subspace composed of the surface atom at $\vec{R}_S$ and the adsorbate at $\vec{R}_a$

$$V^{\sigma}_{\vec{k}n,a} = \sum_{i,\vec{R}_S} c^{\vec{k}n,\sigma}_{i}(\vec{R}_S) V^{\sigma(\text{dim})}_{i\vec{R}_S,a}. \quad (3)$$

The coefficients $c_i^{\vec{k}n,\sigma}(\vec{R}_S)$ are related with the LCAO expansion of the unperturbed $\vec{k}$-surface states,

$$\phi_{\vec{k}n,\sigma}(\vec{r}) = \sum_{i,\vec{R}_S} c_i^{\vec{k}n,\sigma}(\vec{R}_S)\varphi_i(\vec{r} - \vec{R}_S), \tag{4}$$

and they determine the elements of the density matrix of the unperturbed solid given by:

$$\rho_{i,j}^{\sigma}(\vec{R}_S, \vec{R}_{S'}; \varepsilon) = \sum_{\vec{k}n} c_i^{\vec{k}n,\sigma *}(\vec{R}_S) c_j^{\vec{k}n,\sigma}(\vec{R}_{S'}) \delta(\varepsilon - \varepsilon_{\vec{k}n,\sigma}). \tag{5}$$

The number of atoms of the surface contributing to the expansion (4) depends on the magnitude of the atomic hopping integral $V_{i\vec{R}_S,a}^{\sigma(\dim)}$; and the weight of each dimeric contribution is directly related to the band structure through the coefficient $c_i^{\vec{k}n,\sigma}$.

The adsorbate energy level ε_a, calculated by the same procedure, includes the orthogonalization effects and the adsorbate-substrate two-electron interactions considered within a mean field approximation.[25]

This bond-pair model has been able to reproduce, in a quantitative fashion, the main properties of simple homonuclear diatomic molecules such as Li_2, C_2 (Ref. 26). It has also allowed for a general satisfactory description of experimental results in H^+ and Li^+ scattering by a HOPG surface.[27,28] In the last mentioned works the interference terms introduced by the dependence of $V_{\vec{k}n,a}^{\sigma}$ on the $\vec{k}$ component parallel to the surface were neglected.

In summary, for a proper calculation of the atom energy level and the hybridization term $V_{\vec{k}n,a}^{\sigma}$, the bond-pair model requires (i) a good atomic basis set for calculating the one and two electron atomic integrals and (ii) an appropriate description of the surface electronic structure based on a LCAO expansion of the band states.

C. Electronic structure of graphene π band

In a graphene sheet, the carbon atoms are held together via sp^2-hybridized covalent bonds, while the electronic transport takes place by hopping along π orbitals which can participate in covalent bonding with adsorbates. The electrons in the π band of graphene can be described using a tight-binding Hamiltonian within the first-neighbors approximation

$$\hat{H} = -t \sum_{i\in A} \sum_{\vec{\delta}_j (j=1,3)} \frac{1}{V} \sum_{\vec{k},\vec{k}'} [e^{i(\vec{k}-\vec{k}')\cdot\vec{R}_i} e^{-i\vec{k}'\cdot\vec{\delta}_j} \times |\vec{k},A\rangle\langle\vec{k}',B| + \text{H.c.}]. \tag{6}$$

V is the unit cell volume, and the three nearest-neighbor vectors in real space shown in Fig. 1 are given by $\vec{\delta}_1 = \frac{a}{2}(1,\sqrt{3})$; $\vec{\delta}_2 = \frac{a}{2}(1,-\sqrt{3})$; $\vec{\delta}_3 = -a(1,0)$, being $a = 1.42$ Å, and the value of the hopping t is assumed equal to 2.8 eV.[1]

By considering in Eq. (6) the following identity,

$$\frac{1}{V} \sum_{i\in A} e^{i(\vec{k}-\vec{k}')\cdot\vec{R}_i} = \delta(\vec{k} - \vec{k}') \tag{7}$$

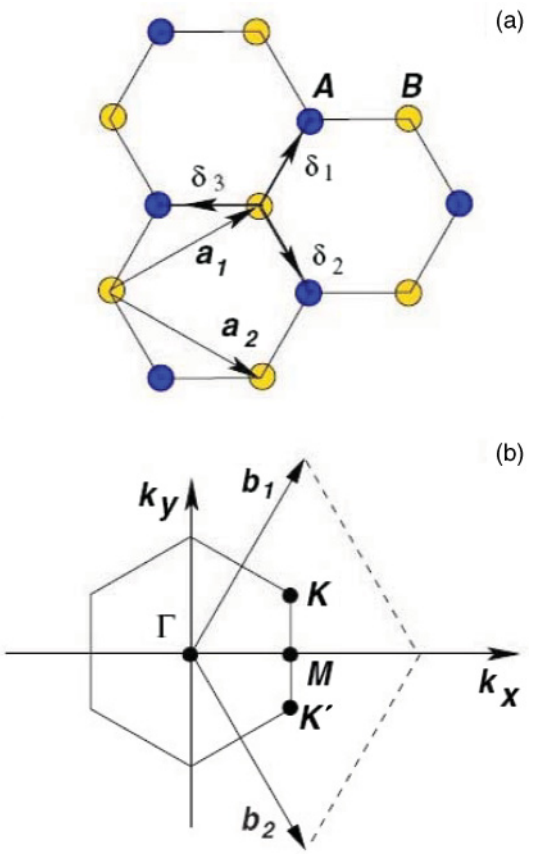

FIG. 1. (Color online) Honeycomb lattice and its Brillouin zone. (a) Lattice structure of graphene, made out of two interpenetrating triangular lattices ($\vec{a}_1 = \vec{\delta}_1 - \vec{\delta}_3$, $\vec{a}_2 = \vec{\delta}_2 - \vec{\delta}_3$ are the primitive vectors). (b) Corresponding Brillouin zone. The Dirac cones are located at the K and K' points.

we arrive to the expression

$$\hat{H} = \sum_{\vec{k}} [\xi_{\vec{k}} |\vec{k},A\rangle\langle\vec{k},B| + \xi_{\vec{k}}^* |\vec{k},B\rangle\langle\vec{k},A|], \tag{8}$$

where the following magnitude has been introduced

$$\xi_{\vec{k}} = -t \sum_{\vec{\delta}_j (j=1,3)} e^{-i\vec{k}\cdot\vec{\delta}_j}. \tag{9}$$

A diagonalization procedure finally gives the energy eigenvalues (introducing now the spin index),

$$\varepsilon_{\vec{k}n,\sigma} = \pm\sqrt{\xi_{\vec{k}}\xi_{\vec{k}}^*}. \tag{10}$$

and the eigenvectors written as a linear combination of atomic p_z orbitals centered on the C atoms of graphene (LCAO expansion)

$$\phi_{\vec{k}n,\sigma}(\vec{r}) = \frac{1}{\sqrt{2N}} \sum_j \left[\pm \frac{\xi_{\vec{k}}}{|\xi_{\vec{k}}|} e^{-i\vec{k}\cdot\vec{R}_j^A} \varphi_{p_z}(\vec{r} - \vec{R}_j^A) + e^{-i\vec{k}\cdot\vec{R}_j^B} \varphi_{p_z}(\vec{r} - \vec{R}_j^B) \right]. \tag{11}$$

In Eqs. (10) and (11) the minus sign applies to the lower bonding-like π band ($n = 1$) and the plus sign to the upper antibonding-like π^* band ($n = 2$).

D. Calculation of the local density of states projected on the adsorbate

The density of states at the adsorbate is calculated as

$$\rho_{a\sigma}(\omega) = \frac{1}{\pi}\mathrm{Im}G_{a\sigma}(\omega). \tag{12}$$

The required Green function,

$$G_{a\sigma}(t,t') = i\Theta(t'-t)\langle\{\hat{c}^{\dagger}_{a,\sigma}(t'),\hat{c}_{a,\sigma}(t)\}\rangle, \tag{13}$$

is solved by using the equations of motion method (EOM) accordingly to the Anderson Hamiltonian [Eq. (1)][34] We used the criterion of closing the EOM by ensuring a strict second-order calculation in the hopping parameter $V^{\sigma}_{\vec{k}n,a}$. Thus, the following expression is found ($\tilde{\omega} = \omega - i\eta$):

$$G_{a\sigma}(\omega) = \frac{1-\langle\hat{n}_{a,\bar{\sigma}}\rangle}{\tilde{\omega}-\varepsilon_a-\Xi_{0\sigma}(\omega)+\frac{U\Xi_{\prec\bar{\sigma}}(\omega)}{\tilde{\omega}-\varepsilon_a-U-\Xi_{0\sigma}(\omega)-\Xi_{1\bar{\sigma}}(\omega)}} + \frac{\langle\hat{n}_{a,\bar{\sigma}}\rangle}{\tilde{\omega}-\varepsilon_a-U-\Xi_{0\sigma}(\omega)+\frac{U[\Xi_{\prec\bar{\sigma}}(\omega)-\Xi_{1\bar{\sigma}}(\omega)]}{\tilde{\omega}-\varepsilon_a-\Xi_{0\sigma}(\omega)-\Xi_{1\bar{\sigma}}(\omega)}}$$
$$+\frac{UI_{\bar{\sigma}}(\omega)}{[\tilde{\omega}-\varepsilon_a-\Xi_{0\sigma}(\omega)][\tilde{\omega}-\varepsilon_a-U-\Xi_{0\sigma}(\omega)-\Xi_{1\bar{\sigma}}(\omega)]+U\Xi_{\prec\bar{\sigma}}(\omega)}, \tag{14}$$

where $\langle\hat{n}_{a,\sigma}\rangle$ is the adatom state occupation per spin and the quantity $I_{\sigma}(\omega)$ has been defined as

$$I_{\sigma}(\omega) = \sum_{\vec{k}n} V^{\sigma *}_{\vec{k}n,a}\frac{\langle\hat{c}^{\dagger}_{a,\sigma}\hat{c}_{\vec{k}n,\sigma}\rangle}{\tilde{\omega}-\varepsilon_{\vec{k}n,\sigma}} - \sum_{\vec{k}n} V^{\sigma}_{\vec{k}n,a}\frac{\langle\hat{c}^{\dagger}_{\vec{k}n,\sigma}\hat{c}_{a,\sigma}\rangle}{\tilde{\omega}+\varepsilon_{\vec{k}n,\sigma}-\varepsilon_A},$$

being $\varepsilon_A = 2\varepsilon_a + U$, and the introduced self-energies are

$$\Xi_{0\sigma}(\omega) = \sum_{\vec{k}n}\frac{|V^{\sigma}_{\vec{k}n,a}|^2}{\tilde{\omega}-\varepsilon_{\vec{k}n,\sigma}},$$
$$\Xi_{\prec\sigma}(\omega) = \sum_{\vec{k}n}|V^{\sigma}_{\vec{k}n,a}|^2\langle\hat{n}_{\vec{k}n,\sigma}\rangle\left[\frac{1}{\tilde{\omega}-\varepsilon_{\vec{k}n,\sigma}}+\frac{1}{\tilde{\omega}+\varepsilon_{\vec{k}n,\sigma}-\varepsilon_A}\right],$$
$$\Xi_{1\sigma}(\omega) = \sum_{\vec{k}n}|V^{\sigma}_{\vec{k}n,a}|^2\left[\frac{1}{\tilde{\omega}-\varepsilon_{\vec{k}n,\sigma}}+\frac{1}{\tilde{\omega}+\varepsilon_{\vec{k}n,\sigma}-\varepsilon_A}\right], \tag{15}$$

In Eq. (15),

$$\langle\hat{n}_{\vec{k}n,\sigma}\rangle = f_{\prec}(\varepsilon_{\vec{k}n,\sigma}) = \frac{1}{1+e^{\frac{\varepsilon_{\vec{k}n,\sigma}-\varepsilon_F}{k_BT}}}, \tag{16}$$

is the Fermi distribution for a temperature T in the case of a metallic surface.

The Green function given by Eq. (14) provides a very appropriate description of the correlated atomic state in the case of a strong Coulomb repulsion U compared with the hybridization width $\Gamma^{\sigma}_{a}(\varepsilon)$ (Ref. 34). It also reproduces correctly the $U = 0$ limit and the isolated atom case $V = 0$.

III. RESULTS AND DISCUSSION

A. Hamiltonian terms

We used the atomic basis set for C and Li atoms provided by Huzinaga *et al.*,[35,36] including a p polarization function in the case of Li.

In Fig. 2 the ionization and affinity levels of Li, measured with respect to the Fermi level, are shown as a function of the normal distance (z) to the surface. They are obtained as the difference between the total energies of the system with $N+1$ and N electrons calculated without allowing charge exchange.[28] The correct assymptotic values of -5.39 and 0.6 eV with respect to the vacuum level are recovered for the ionization and affinity levels, respectively. The effect of the long-range interactions is introduced by considering the image potential defining the behavior of the energy level for large normal distances. We can see from Fig. 2 that the effective Coulomb repulsion U in the atomic state is reduced to values around 2 eV near the surface. The energy levels for two

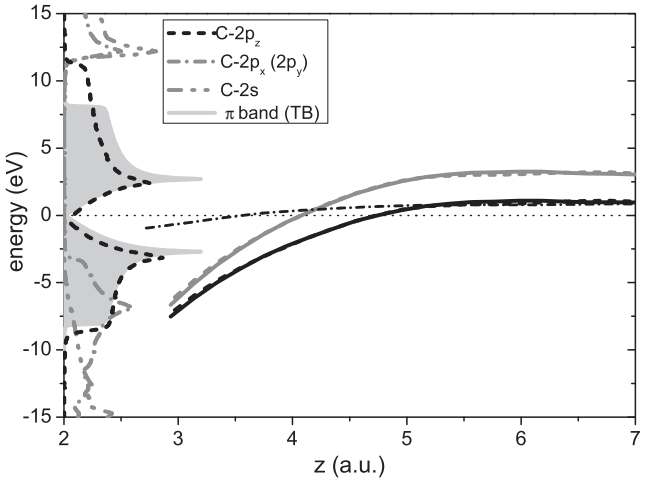

FIG. 2. Energy levels of Li atom as a function of the distance to the surface. Black (grey) lines are the ionization (affinity) level. Solid line for the adatom placed on top of a carbon atom and dash line for the adatom located on the center of an hexagon. The dot-dash line is the ionization level by considering the interaction with only the nearest C atom in the on top position. The shadowed region is the LDOS of the π band calculated in this work. It is also shown the s and p LDOS of graphene calculated as in Refs. 37 and 38. The energies are referred to the Fermi energy set equal to 0.

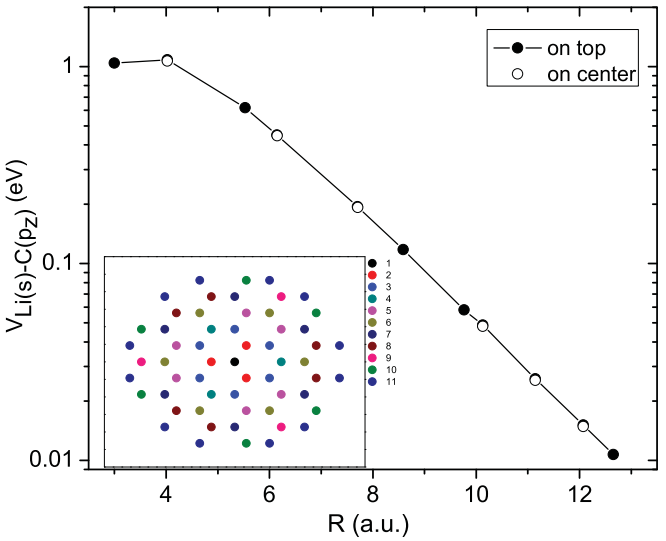

FIG. 3. (Color online) The hopping term $V_{Li(s)-C(pz)}$ as a function of the distance (R) between the Li atom at $z = 3$ a.u. and the C atoms of the successive neighbor shells on the surface (see inset). Full circles correspond to the on-top position and empty symbols to the on-center position.

adsorption sites are depicted: the adatom placed either on top of a carbon atom or located in the center of an hexagon. In the same figure we show the evolution of the ionization level when the interaction with only one surface atom is considered. The comparison between both evolutions shows the importance of considering the interaction with all the surface atoms that the adatom can "see." The downshift of the energy level close to the surface is due to the interaction with several atoms of the solid, originated in the extension of the Li atomic states, and the rather compact spatial distribution of C atoms in graphene. The energy level variation is finally determined by a detailed balance between attractive and repulsive terms.

The atomic coupling between the Li-2s and C-2p_z states [$V_{Li(s)-C(p_z)}$] is shown in Fig. 3 as a function of the distance between the Li atom positioned at $z = 3$ a.u. and the carbon atoms belonging to the different neighbor shells on the surface (first, second, and so on). In the on-top position the coupling with one atom of the 11th neighbor shell is 100 times smaller than the one with the first neighbor.

The $|V^{\sigma}_{\vec{k}n,a}|^2$ calculated as

$$|V^{\sigma}_{\vec{k}n,a}|^2 = \left| \frac{1}{\sqrt{2}} \sum_j \left[\pm \frac{\xi_{\vec{k}}}{|\xi_{\vec{k}}|} e^{-i\vec{k}\cdot\vec{R}^A_j} V_{Li(s)-C(p_z)}(\vec{R}^A_j) + e^{-i\vec{k}\cdot\vec{R}^B_j} V_{Li(s)-C(p_z)}(\vec{R}^B_j) \right] \right|^2, \quad (17)$$

is shown in Fig. 4 as a function of the modulus of $\vec{k}$ for the case of Li on top. It is compared with the calculation including the interaction only with the C atom below the Li, and the one including the four nearest carbons. The results for the two bands are depicted, being also included the energy band structure given by Eq. (10).

It can be noticed from Fig. 4 the remarkable peaked structure of $|V^{\sigma}_{\vec{k}n,a}|^2$ around the Γ point in the case of the

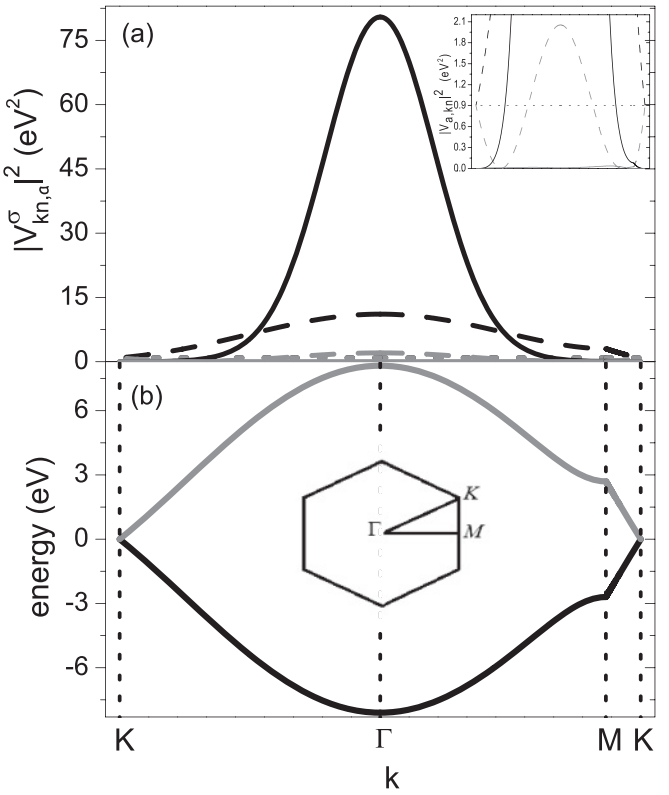

FIG. 4. (a) The square modulus of $V^{\sigma}_{\vec{k}n,a}$ [Eq. (17)] as a function of $|\vec{k}|$ for the Li on top at $z = 3.6$ a.u. Black lines correspond to the valence band $n = 1$, and grey lines to the conduction band $n = 2$. Calculation including all the C atoms that are capable of interacting (solid lines); the one including the four nearest neighbors (dashed line); and the calculation including only the C below the Li atom (dotted line). The inset is a blow up to show the results for $n = 2$. (b) The band energies $\varepsilon_{\vec{k}n,\sigma}$ as a function of $|\vec{k}|$ [Eq. (10)].

valence band $n = 1$, when all the C atoms that can interact with Li are included. The inclusion of only the four nearest-neighbor carbons leads to a more extended function in $|\vec{k}|$ which is approximately five times smaller at $|\vec{k}| = 0$. In the case of the antibonding-like band $n = 2$ a practically negligible $|V^{\sigma}_{\vec{k}n,a}|^2$ is found for any value of $|\vec{k}|$. This result is better seen in Fig. 5 where contour plots of $|V^{\sigma}_{\vec{k}n,a}|^2$ are shown for the two bands ($n = 1, 2$). In the case of $n = 2$ the negligible values show a maximum near the M points (in the paths from Γ to M).

The observed behavior of $|V^{\sigma}_{\vec{k}n,a}|^2$ when many C atoms are involved in the interaction with the adatom tends to the limit behavior obtained in the case of a very large number of C atoms interacting with similar coupling values. By assuming in Eq. (17) $V_{Li(s)-C(p_z)}(\vec{R}^{A,B}_j) \approx V_a$ and using the identity given by Eq. (7), we obtain

$$|V^{\sigma}_{\vec{k}n,a}|^2 \equiv \frac{V_a^2}{2} |V\delta(\vec{k})[\mp 1 + 1]|^2.$$

In this very extreme limit situation we have that $|V^{\sigma}_{\vec{k}n,a}|^2$ is zero in the case of the antibonding $n = 2$ band, while it becomes a delta function in $\vec{k} = 0$ for the bonding-like band. In what follows we will see how these features are reflected in the energy dependence of the hybridization width.

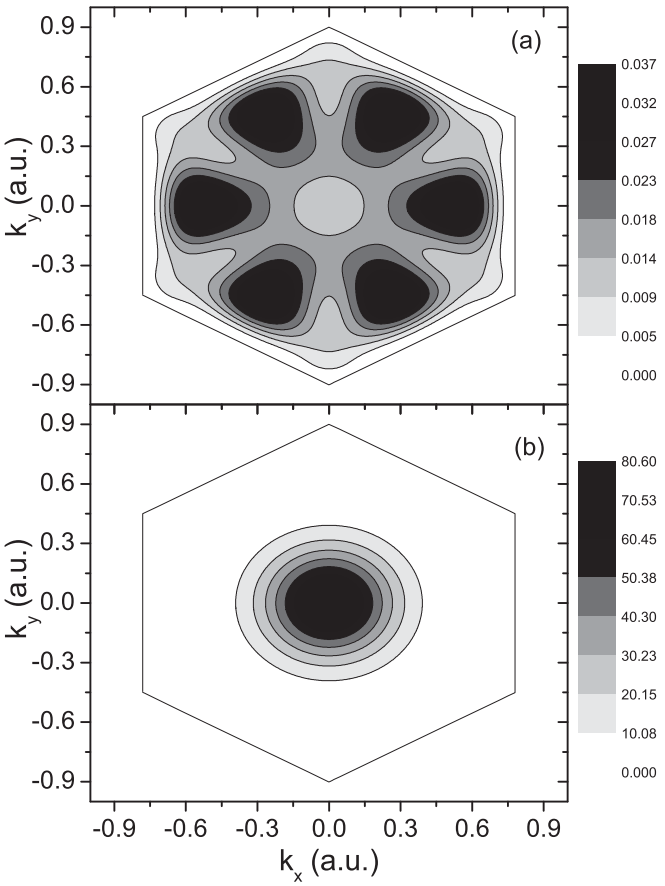

FIG. 5. Surface contour plot of $|V^{\sigma}_{\vec{k}n,a}|^2$ as a function of the $\vec{k}$ components, for Li on top at $z = 3.6$ a.u. The grey scale is used to indicate the variation of the square modulus of $V^{\sigma}_{\vec{k}n,a}$. (a) Conduction band $n = 2$ and (b) valence band $n = 1$.

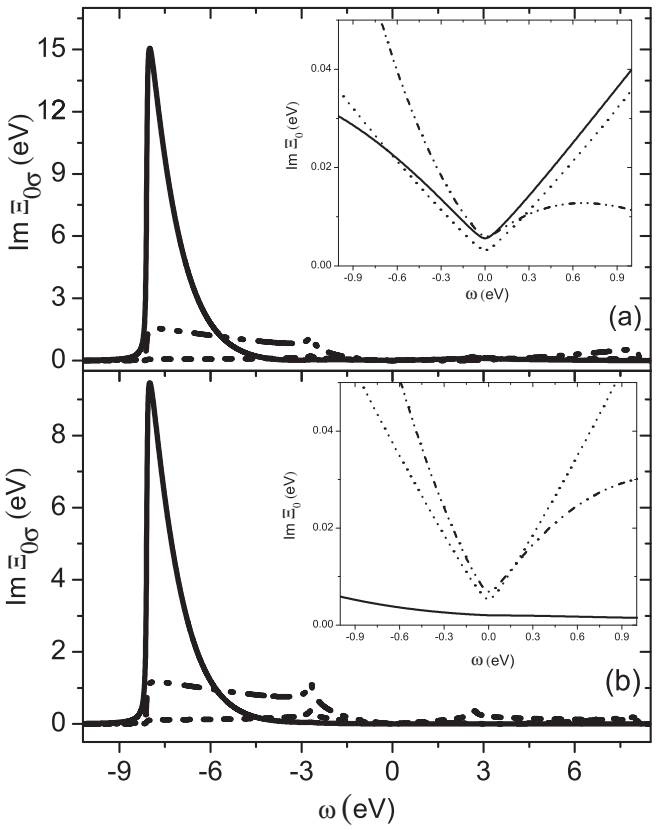

FIG. 6. The hybridization width as a function of energy in the case of Li on top of a C atom for two normal distances to the surface: (a) $z = 3$ a.u., (b) $z = 6$ a.u.. Solid line includes the interaction with all the surface atoms which are able of coupling; dashed-dot-dot line to the interaction with the four nearest C atoms, and dashed line to the interaction with only the C atom below the Li. In the inset the details around the Fermi level ($\varepsilon_F = 0$) are shown.

B. Hybridization width

Figures 6 and 7 show $\Gamma^{\sigma}_{a}(\omega) = \mathrm{Im}\Xi_{0\sigma}(\omega)$ for the Li atom either on top of a carbon atom or in the center of an hexagon at different normal distances z to the surface.

In all cases the hybridization width presents a pronounced maximum at the bottom of the valence band ($\omega \approx \varepsilon_{\vec{k}=0,n=1}$) when all the neighbor atoms that interact effectively with Li are included. The narrow function decreases rapidly for increasing energies accordingly to the $|V^{\sigma}_{\vec{k}n,a}|^2$ behavior and the energy gap between the bonding and antibonding band states (see Fig. 4). Very small values of the hybridization width in the vicinity of the Dirac point are found in all the cases. The proportionality of $\Gamma^{\sigma}_{a}(\omega)$ to the LDOS of graphene is ensured either in the case of considering the interaction with only one C atom (the nearest one in the on-top position), or by disregarding the interference between the quantum mechanical paths involving the different neighboring sites. For the Li on top at 3 a.u. it can be observed [inset of Fig. 6(a)] a linear dependence of $\Gamma^{\sigma}_{a}(\omega)$ with energy only very close to the Fermi level. However, at 6 a.u. this linear energy dependence is lost when including all the C atoms which effectively interact. The differences observed are due to the distance behavior of the coupling term shown in Fig. 3. Note that, in the case of Li at 3 a.u., the coupling with the first neighbor is practically the same as the one with the second neighbors.

In the symmetric case, the Li atom in the center of a hexagon, the inclusion of only the six nearest C atoms leads to a hybridization width that scales with $|\omega|^3$ for energy values close to the Fermi energy[18] [insets of Figs. 7(a) and 7(b)]. This broadening function becomes even more anomalous when the effective coupling between the adatom and the surface atoms extends far away from the first neighbors, as can be observed in Fig. 7. We can see from Figs. 6 and 7 that at $z = 6$ a.u. the hybridization widths for the on-top and the on-center adsorption sites do not differ substantially if all the active neighbors are considered. We found that this is, in general, true for normal distances larger than 4 a.u., for which the atomic coupling term is a monotonous decreasing function of distance in both cases (see Fig. 3). Hence, the broadening of the adatom ionization level given by $\Gamma^{\sigma}_{a}(\varepsilon_a)$ in both adsorption sites is very similar, as is observed in Fig. 8. In the same figure the level broadening is depicted in the case of considering only the nearest C atom in the on-top position, which results to be nearly six times larger for $z > 4$ a.u. In Fig. 8 we include for comparison the calculation of $\Gamma^{\sigma}_{a}(\varepsilon_a)$ by disregarding the interference between the different paths involving the neighboring sites. We can see that this calculation overestimates notably (by orders of magnitude) the level width for large distances.

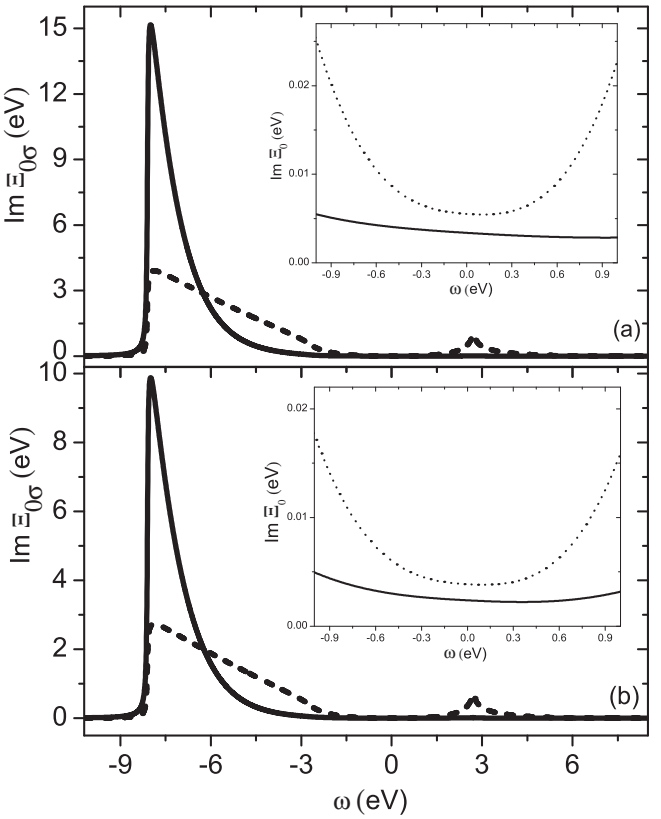

FIG. 7. The hybridization width as a function of energy in the case of Li on the center of an hexagon of C atoms for two normal distances to the surface: (a) $z = 3$ a.u., (b) $z = 6$ a.u. Solid line includes the interaction with all the surface atoms which are able of coupling, dashed line to the interaction with the six nearest C atoms. In the inset the details around the Fermi level ($\varepsilon_F = 0$) are shown.

All the peculiarities observed have their origin in the strong localization of $|V^{\sigma}_{\vec{k}n,a}|^2$ and the pronounced energy gap around $\vec{k} = 0$. On the other hand, this fact is related to the interaction of Li with several atoms provided the extension of the Li-2s and C-2p_z atomic states. Therefore, the hybridization widths are strongly dependent on the symmetry and range of the atom-atom interactions.

In Fig. 9 we compare the hybridization widths for the cases of Li-2s and Li-2p_y states. It is observed that the hybridization width is a function more extended in energy with larger values around the Fermi level in the case of the interaction with Li-2p_y state [inset in Fig. 9(a)]. This is an expected result taking into account that the coupling with all the C atoms located at $x = 0$ is inhibited by symmetry, leading in this form to a less localized hybridization term at $\vec{k} = 0$. Accordingly to this analysis, one concludes that the excited state of Li should be considered for a more correct description of the interaction with graphene.

C. Local density of states on the adatom and valence occupation

All the calculations here are performed by considering $T = 0K$. The strongly reduced hybridization in a wide range of energy values leads to very narrow resonances in the local density of states $\rho_{a\sigma}(\omega)$ [Eq. (14)], as we can see in Fig. 10(a) for the case of Li on the center of the hexagon ($z = 4$ a.u.). The

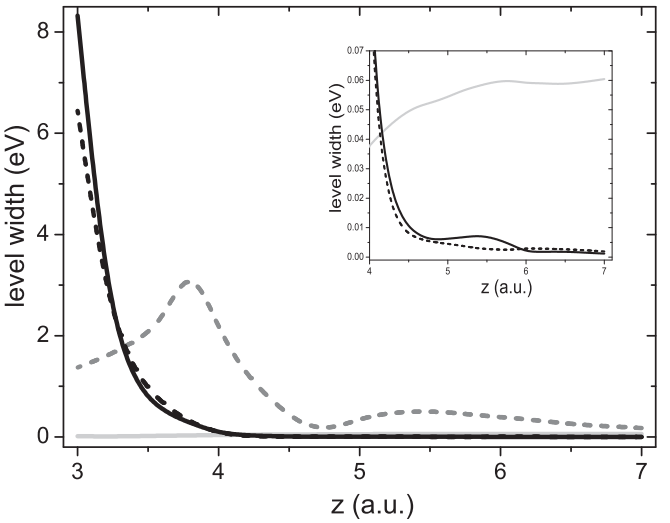

FIG. 8. The ionization level half-width (the hybridization width evaluated in the atom energy level) as a function of normal distance to the surface: black solid line corresponds to the on top position, and black dashed line to the on center one. Grey solid line is the calculation by considering only the nearest C atom in the on top adsorption site; grey dashed line is the calculation with all the active carbons but disregarding the interference between the different paths involving the neighboring sites. A blow up of the large distance behavior is shown in the inset.

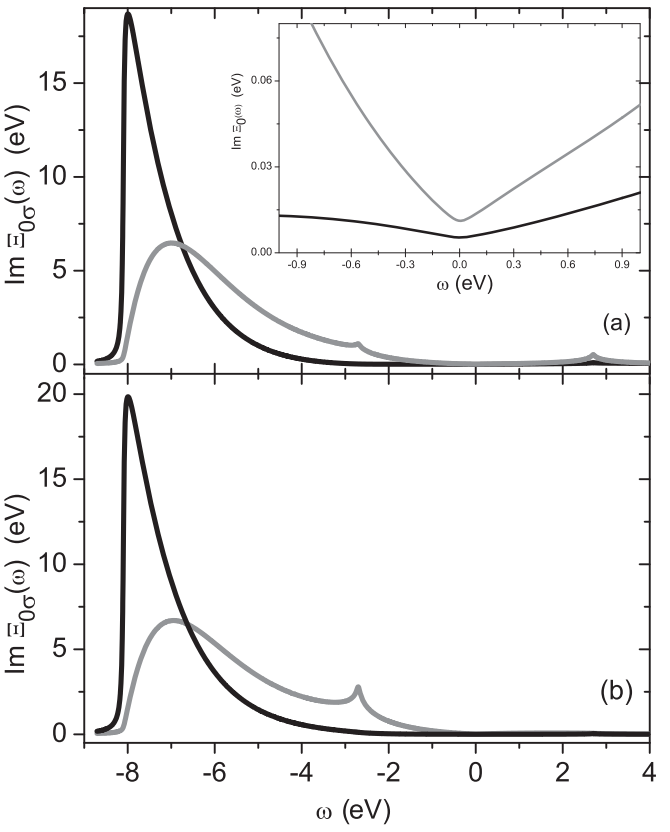

FIG. 9. Hybridization widths as a function of energy for the Li-2s (black line) and Li-2p_y (grey line) at a distance $z = 3$ a.u. (a) On top and (b) on center of the hexagon adsorption sites. The inset in (a) shows the details around the Fermi level.

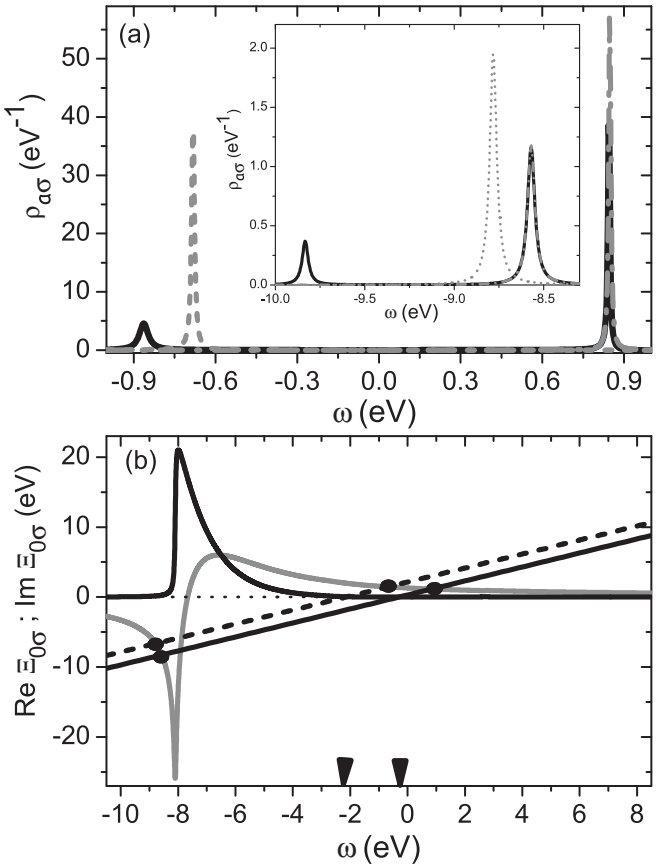

FIG. 10. (a) Local density of states on the adatom as a function of energy in the case of Li at 4 a.u. in the on-center position: black solid line corresponds to finite U, and grey lines to $U = 0$ by considering either the ionization level (dashed line) or the affinity level (dot-dashed line). In the inset: the resonances at the bottom of the valence band. (b) The real (grey line) and the imaginary (black line) parts of $\Xi_{0\sigma}(\omega)$. The straight lines correspond to $\omega - \varepsilon_a$(dashed line) and to $\omega - \varepsilon_a - U$ (solid line); the position of the resonances are indicated by black circles, and the black arrows indicate the ionization and affinity energies of Li at this distance from the surface.

$U = 0$ calculation by considering either the ionization level or the affinity one is also shown in the same figure. Both finite and zero U calculations show similar trends in the evolution of the adatom s-state occupation; only slight differences are found in the case of the resonance energy positions. Additional resonances appear at the bottom and out of the valence band ($\omega \leqslant -8.4$ eV) [see inset of Fig. 10(a)] due to the smooth fall down to zero of $\mathrm{Im}\,\Xi_{0\sigma}(\omega)$ and the energy behavior of $\mathrm{Re}\,\Xi_{0\sigma}(\omega)$ shown in Fig. 10(b). In this sense a non-Markovian environment is controlling the decay dynamics of the local excitation in this case, where a "quantum diffusion" described by a return term brings out the details of the spectral structure of the environment.[39,40]

Anderson showed that when ε_a is below the Fermi energy ε_F and the energy of the doubly occupied state $\varepsilon_a + U$ is larger than ε_F, a magnetic state is possible if U is sufficiently large and/or Γ_a^σ sufficiently small.[29] In the case of Li interacting with graphene the requirement of a hybridization width small enough to allow for a magnetic state is fulfilled. The evolution

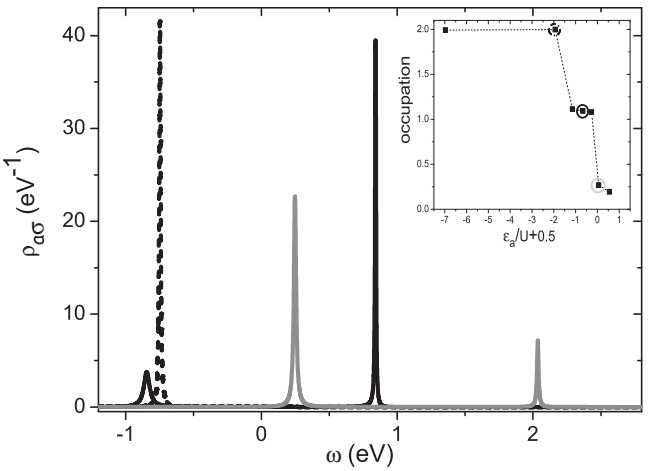

FIG. 11. The local density of states on the Li atom located at the on top position at distance values $z = 3.6$ a.u. (black dashed line), 4 a.u. (black solid line), and 4.4 a.u. (grey solid line). In the inset: occupation of Li state as a function of $\varepsilon_a/U + 0.5$.

with distance of the local density of states in the on top adsorption geometry is shown in Fig. 11. It can be observed in the inset that a local magnetic moment exists for $-2.4 < \varepsilon_a/U < -0.44$, which corresponds to 3.6 a.u. $< z <$ 4.4 a.u.. Electronic transport measurements performed in this very weakly coupled system would show a typical Coulomb blockade behavior.

D. Neutral fraction in ion scattering

In the case of Li^+ scattering by a graphene surface, the neutral fraction is calculated by using the time-dependent Green function formalism in the $U = 0$ limit.[28]

In dynamical ion-surface scattering processes we are interested in calculating the probability of ion neutralization. Within the spinless approximation, this is given by the time-dependent average atom state occupation $\langle n_a(t)\rangle = \langle c_a^\dagger(t)c_a(t)\rangle$. This quantity is obtained from the following Green function at equal time values:

$$F_{aa}(t,t') = i\langle\Phi|[c_a^\dagger(t'),c_a(t)]|\Phi\rangle \rightarrow i[2\langle n_a(t)\rangle - 1]_{t\rightarrow t'},$$

where [ ] indicates the commutator, and Φ is the dynamical state in the Heisenberg picture.

In the present calculation the ion trajectory $z = z(t)$ is assumed normal to the surface with a turning point chosen at a distance of 3 a.u. to involve only the π band in the scattering process. The ingoing and exit velocity values are equal to the corresponding normal components of the experimental setup. The scattering angle in the experiment is equal to 45°, and the projectile kinetic energy is 2 keV.[28] The neutral fraction is shown in Fig. 12(a) as a function of the exit angle measured respect to the surface plane. The Li^+ ions are partially neutralized close to the surface due to the downshift of the ionization energy (Fig. 2). The level width is strongly reduced at large distances when the contribution of all the active C atoms is considered [Fig. 12(b)]. This suppresses the electron loss far from the surface leading to either a constant or an increasing neutral fraction at low velocities. In Fig. 12(a)

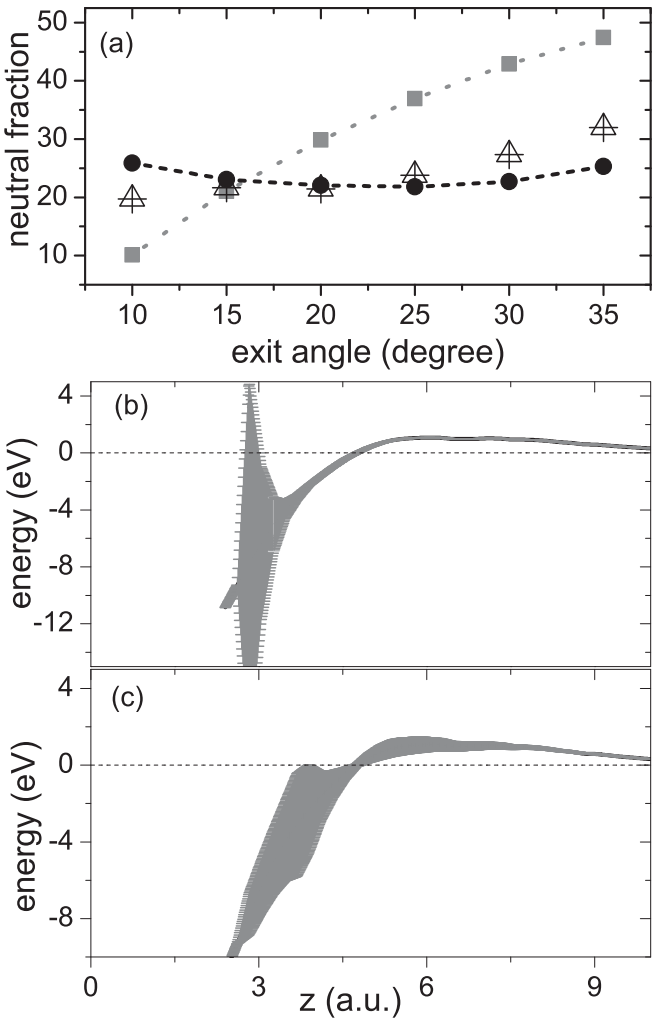

FIG. 12. (a) Full circles are the neutral fraction calculated by considering the C-C interference terms, while the full squares are the calculation by disregarding the interference terms. The crossed triangles are the experimental data of Ref. 28 obtained for 2 keV Li^+ scattering by a HOPG surface (scattering angle equal to 45°). (b) The energy level and its width shown as error bars in the case of including correctly the interaction with all the active C atoms; (c) the same as in (b) but disregarding the interference between C atoms.

we show the calculation in which we neglect the interferences between the C atoms interacting with the Li^+ projectile. In this case the neutral fraction falls down at low velocities because the level broadening is large enough to allow for a more efficient electron loss process as the ion velocity decreases [see Fig. 12(c)]. The experimental values of the Li neutral fraction correspond to a HOPG surface whose crystal structure is basically a staggered arrangement of C atoms in weakly coupled parallel layers of graphene. Nevertheless, at low exit energies the charge state of the projectile is defined far from the surface and only the C atoms of the surface layer and the π band are involved (see Fig. 2). Therefore, the suppression of the hybridization width found in the case of Li interacting with the π band of graphene can explain the nearly constant neutral fraction measured for small exit angles in the Li^+ scattering by HOPG.

IV. CONCLUSION

We have studied the interaction of an Li atom with graphene by using the Anderson model and an *ab initio* calculation of the hybridization term. In this form, the chemical properties of the interacting atoms and the two dimensional features of the graphene band structure are properly accounted for. We find that the interaction of Li with graphene involves several atoms of the solid due to the extension of the Li-2s and C-2p_z atomic states, and the rather compact spatial distribution of C atoms in the surface. In consequence, the hybridization width is found to be a peaked function at the bottom band energy which decays rapidly to negligible values for larger energies. In addition, the level broadening is not strongly dependent on the adsorption site, and a local magnetic moment formation is possible within this very weak coupling regime. Furthermore, the high neutralization measured in low energy ion scattering experiments can also be explained by the negligible hybridization width around the Dirac point. Thus, we conclude that the spectral features of atoms interacting with graphene are determined by the symmetry and chemical properties of the involved atomic states, and the energy gap of the π band structure.

ACKNOWLEDGMENTS

We acknowledge helpful discussions with Horacio Pastawski and Fernando Flores. The authors also thank F. Flores and V. H. Ponce for a critical reading of the manuscript. This work was supported by ANPCyT through PICT-07-0811 and U.N.L. through CAI+D grants.

[1] A. H. C. Neto, F. Guinea, N. M. R. Peres, K. S. Novoselov, and A. K. Geim, Rev. Mod. Phys. **81**, 109 (2009).
[2] V. Geringer, M. Liebmann, T. Echtermeyer, S. Runte, M. Schmidt, R. Rückamp, M. C. Lemme, and M. Morgenstern, Phys. Rev. Lett. **102**, 076102 (2009).
[3] G. Li, A. Luican, and E. Y. Andrei, Phys. Rev. Lett. **102**, 176804 (2009).
[4] Y. Zhang, V. W. Brar, F. Wang, C. Girit, Y. Yayon, M. Panlasigui, A. Zettl, and M. F. Crommie, Nature Phys. **4**, 627 (2008).
[5] D. M. Eigler and E. K. Schweizer, Nature (London) **344**, 524 (1990).
[6] K. Sengupta and G. Baskaran, Phys. Rev. B **77**, 045417 (2008).
[7] B. Uchoa, V. N. Kotov, N. M. R. Peres, and A. H. Castro Neto, Phys. Rev. Lett. **101**, 026805 (2008).
[8] M. Khantha, N. A. Cordero, L. M. Molina, J. A. Alonso, and L. A. Girifalco, Phys. Rev. B **70**, 125422 (2004).
[9] K. T. Chan, J. B. Neaton, and M. L. Cohen, Phys. Rev. B **77**, 235430 (2008).

[10]T. O. Wehling, M. I. Katsnelson, and A. I. Lichtenstein, Chem. Phys. Lett. **476**, 125 (2009).
[11]A. V. Krasheninnikov, P. O. Lehtinen, A. S. Foster, P. Pyykko, and R. M. Nieminen, Phys. Rev. Lett. **102**, 126807 (2009).
[12]L. Hu, X. Hu, X. Wu, C. Du, Y. Dai, and J. Deng, Physica B **405**, 3337 (2010).
[13]T. O. Wehling, H. P. Dahal, A. I. Lichtenstein, M. I. Katsnelson, H. C. Manoharan, and A. V. Balatsky, Phys. Rev. B **81**, 085413 (2010).
[14]R. E. Mapasha and N. Chetty, Comput. Mater. Sci. **49**, 787 (2010).
[15]P. A. Khomyakov, G. Giovannetti, P. C. Rusu, G. Brocks, J. van den Brink, and P. J. Kelly, Phys. Rev. B **79**, 195425 (2009).
[16]Y. Yagi, T. M. Briere, M. H. F. Sluiter, V. Kumar, A. A. Farajian, and Y. Kawazoe, Phys. Rev. B **69**, 075414 (2004).
[17]P. S. Cornaglia, G. Usaj, and C. A. Balseiro, Phys. Rev. Lett. **102**, 046801 (2009).
[18]B. Uchoa, L. Yang, S.-W. Tsai, N. M. R. Peres, and A. H. Castro Neto, Phys. Rev. Lett. **103**, 206804 (2009).
[19]T. O. Wehling, H. P. Dahal, A. I. Lichtenstein, M. I. Katsnelson, H. C. Manoharan, and A. V. Balatsky, Phys. Rev. B **81**, 085413 (2010).
[20]T. B. Grimley, Proc. Phys. Soc. London **90**, 751 (1967).
[21]T. B. Grimley, Proc. Phys. Soc. London **92**, 776 (1967).
[22]T. B. Grimley, J. Phys. C **3**, 1934 (1970).
[23]D. M. Newns, Phys. Rev. B **178**, 1123 (1969).
[24]P. G. Bolcatto, E. C. Goldberg, and M. C. G. Passeggi, Phys. Rev. A **50**, 4643 (1994).
[25]P. G. Bolcatto, E. C. Goldberg, and M. C. G. Passeggi, Phys. Rev. B **58**, 5007 (1998).
[26]J. O. Lugo, L. I. Vergara, P. G. Bolcatto, and E. C. Goldberg, Phys. Rev. A **65**, 022503 (2002).
[27]F. Bonetto, M. A. Romero, E. A. García, R. Vidal, J. Ferrón, and E. C. Goldberg, Europhys. Lett. **80**, 53002 (2007).
[28]F. Bonetto, M. A. Romero, E. A. García, R. A. Vidal, J. Ferrón, and E. C. Goldberg, Phys. Rev. B **78**, 075422 (2008).
[29]P. W. Anderson, Phys. Rev. **124**, 41 (1961).
[30]A. R. Canario, T. Kravchuk, and V. Esaulov, New J. Phys. **8**, 22 (2006).
[31]A. R. Canario, A. G. Borisov, J. P. Gauyacq, and V. A. Esaulov, Phys. Rev. B **71**, 756 121401 (2005).
[32]A. Iglesias-García, E. A. Garcia, and E. C. Goldberg, J. Phys. Condens. Matter **23**, 045003 (2011).
[33]P. O. Lowdin, J. Chem. Phys. **18**, 365 (1950).
[34]M. A. Romero, F. Flores, and E. C. Goldberg, Phys. Rev. B **80**, 235427 (2009).
[35]S. Huzinaga, J. Chem. Phys. **42**, 1293 (1965).
[36]*Gaussian Basis Set for Molecular Calculation*, edited by S. Huzinaga (Elsevier, Amsterdam, 1984).
[37]J. P. Lewis, K. R. Glaesemann, G. A. Voth, J. Fritsch, A. A. Demkok, J. Ortega, and O. F. Sankey, Phys. Rev. B **64**, 195103 (2001).
[38]P. Jelinek, H. Wang, J. P. Lewis, O. F. Sankey, and J. Ortega, Phys. Rev. B **71**, 235101 (2005).
[39]A. D. Dente, R. A. Bustos-Marún, and H. M. Pastawski, Phys. Rev. A **78**, 062116 (2008).
[40]E. Rufeil-Fiori and H. M. Pastawski, Physica B **404**, 2812 (2009).